Integrating AHP and machine learning for flood hazard mapping: Evaluating land use planning effectiveness in Ha Tinh, Vietnam

Le Van PHU[1], Trinh Le HUNG[2,*], Khuong Van LONG[1], Nguyen Dinh HAI[1]

[1] Vietnam People Naval Hydrographic and Oceanographic Department, Haiphong, Vietnam
[2] Le Quy Don Technical University, Hanoi, Vietnam
*Corresponding author e-mail address: trinhlehung@lqdtu.edu.vn

Received: 25 January 2026 / Accepted: 23 September 2026

Abstract. Flooding is among the most destructive natural hazards in Central Vietnam, causing recurrent damage to infrastructure, rural livelihoods, and ecosystems. This study presents an integrated multi-criteria framework coupling the Analytic Hierarchy Process (AHP) with a Support Vector Machine (SVM) algorithm to refine flood hazard zoning and assess spatial conflicts within the 2030 land use master plan of Ha Tinh province. Six conditioning indicators, proximity to stream, slope, elevation, aspect, land use/land cover, and precipitation, were evaluated and weighted through expert consensus. To resolve the spatial fragmentation typical of linear index overlay, an SVM model with a Radial Basis Function (RBF) kernel was trained on contrastive samples derived from the extreme hazard tiers of the baseline AHP map. The machine learning model demonstrated strong spatial consistency and generalization capability relative to the expert-derived baseline, achieving an Overall Accuracy (OA) of 92.5% and a Kappa coefficient of 0.85 on the validation sample set. Rather than acting as an empirical predictive model against historical inundation events, this workflow operates as a self-referencing spatial optimization tool that effectively smooths rigid, linear classification thresholds into continuous susceptibility gradients. The flood risk map indicated that nearly two-thirds of the province is classified as high or very high flood risk, with the "very high risk" zone alone covering 2840.24 km² (47.66%) and the "high risk" zone 1,027.40 km² (17.24%). Spatial overlay with the provincial 2030 land use plan reveals that 4,100.65 km² of planned land intersects high and very high flood hazard zones, including 2,412.12 km² of forest land, 622.83 km² of paddy land, and 613.77 km² of designated residential areas. These findings demonstrate significant spatial exposure in future development zones, providing actionable spatial evidence to integrate non-structural risk zoning and climate adaptation strategies into long-term territorial planning.

Keywords: Flood hazard, machine learning, Support Vector Machine, land use planning.

1. Introduction

Flooding is widely recognized as one of the most destructive natural hazards globally, posing significant threats to human life, property, agriculture, and ecosystems (Jonkman, 2005; Kundzewicz et al., 2013; Glago, 2021). According to international disaster reports, floods account for a large proportion of natural disaster related damages each year, not only in terms of economic losses but also in terms of social disruption and environmental degradation (Dobrovičová et al., 2015; Istomina & Dobrovoski, 2016). In developing countries, the consequences are often more severe due to limited infrastructure, insufficient early-warning systems, and rapid population growth in flood-prone areas (Perera et al., 2020, Kiptum et al., 2025; Ringo et al., 2025).

Vietnam, located in a tropical monsoon climate zone, is highly vulnerable to hydro-meteorological hazards, particularly floods (Hoang et al., 2019; Nguyen et al., 2021). The North Central Coast, where Ha Tinh province is situated, experiences heavy seasonal rainfall, frequent typhoons, and complex river systems that make the region prone to recurrent flooding (Pham et al., 2018; Ortiz-Vargas & Sebesvari, 2021). Historical records indicate that Ha Tinh has suffered multiple large-scale flood events over recent decades, causing substantial damage to infrastructure, agriculture, and local livelihoods (Le et al., 2021; Nguyen, 2023). The province's geographical characteristics, including mountainous areas in the west and low-lying plains along the coast, further increase its exposure to flood hazards (Le et al., 2023; Nguyen et al., 2023). In Central Vietnam, flood management and land governance face profound institutional challenges, requiring flexible planning frameworks capable of adapting to shifting hydro-meteorological extremes (Nguyen et al., 2023). Furthermore, addressing these territorial vulnerabilities demands a systematic integration of natural landscape triggers and socio-economic exposure parameters to enhance community resilience (Nguyen, 2023; Odiana et al., 2026).

Rapid socio-economic development has also contributed to the intensification of flood risks (Gu et al., 2020; Yin et al., 2021; Ullah et al., 2025). The expansion of industrial zones, infrastructure projects, and urban areas has led to significant land-use changes, reducing natural water retention capacity and increasing surface runoff (Xu et al., 2020; Bojer et al., 2025). This dynamic underscores how expanding human footprints and unguided land use conversions aggravate disaster hazards by disrupting natural catchment hydrology (Millimono, 2026). In coastal central provinces, local spatial planning frequently collides with climate-driven flood risks, underscoring the necessity of mainstreaming ecosystem-based disaster reduction into statutory land allocation (Tran et al., 2009). At the same time, climate change is projected to intensify rainfall extremes and sea-level rise, which are likely to exacerbate flood frequency and severity in the coming decades (Kirshen et al., 2008; Goodess, 2013; Rajkhowa & Sarma, 2021). These combined natural and anthropogenic pressures underline the urgent need for comprehensive flood risk assessment in the province (Le et al., 2021; Loi et al., 2022), highlighting the critical relevance of adapting long-term territorial planning to climate-induced hazards for sustainable regional resource management (Donn-Arnold et al., 2026).

In recent years, advances in remote sensing and Geographic Information Systems (GIS) have provided new opportunities for flood risk mapping (Dano Umar et al., 2011; Wang & Xie, 2018; Amatebelle et al., 2025). The Analytic Hierarchy Process (AHP) has been widely applied as a multi-criteria decision-making approach to assign weights to various flood-related indicators, producing expert-driven risk maps (Ghosh & Kar, 2018; Goumghar et al., 2025; Singha et al., 2025). However, while AHP is transparent and systematic, it is also subjective and may not fully capture complex, nonlinear interactions between indicators (Munier & Hontoria, 2021). In contrast, machine learning algorithms have demonstrated strong capabilities in classification and prediction, allowing for data-driven modeling of flood susceptibility (Zhou et al., 2023; Al-Kindi & Alabri, 2024).

Although the integration of multi-criteria decision analysis (e.g., AHP) and machine learning (ML) has gained global attention, its explicit deployment to evaluate the spatial efficacy and disaster conflicts of official land use master plans remains distinctly underdeveloped in Central Vietnam. Prior flood hazard assessments in Ha Tinh province have predominantly relied on either standalone expert-based weighting models or purely data-driven classification algorithms.

Traditional AHP approaches often introduce subjective judgment and generate fragmented, step-like risk boundaries due to linear summation, which oversimplifies complex hydro-geomorphic interactions. Conversely, data-driven machine learning models in this region are frequently constrained by the scarcity of systematically georeferenced historical flood inventories. More importantly, existing studies typically conclude at hazard delineation without translating spatial hazard surfaces into practical evaluation instruments for statutory land allocation, such as the provincial 2030 land use master plan. Consequently, a pronounced research gap exists regarding how an integrated, self-referencing AHP-ML workflow can bridge expert criteria and continuous spatial modeling to rigorously cross-examine future land allocation vulnerabilities under escalating climate risks.

To address this gap, this study presents an integrated framework that couples AHP-derived multi-criteria evaluation with a Support Vector Machine (SVM) classifier to optimize flood hazard mapping and appraise the 2030 land use plan of Ha Tinh province. We formulate the central research hypothesis that a supervised machine learning classifier (SVM with an RBF kernel), trained on high-contrast terminal hazard classes derived from expert knowledge, can successfully overcome the rigid, linear decision boundaries of traditional AHP. Specifically, we hypothesize that this non-linear kernel transformation can filter local boundary noise, smooth spatial fragmentation, and generalize continuous flood susceptibility gradients across complex topographic gradients without requiring exhaustive empirical inundation inventories. By overlaying the resulting continuous hazard surfaces onto the official 2030 land use plan, this study seeks to provide objective, spatially explicit evidence to identify structural exposure hotspots, prevent misallocated socio-economic development, and support climate-resilient territorial governance in Central Vietnam.

2. Materials and methods

2.1. Study area

The study was conducted in Ha Tinh province, located in the North Central of Vietnam (Fig. 1). Ha Tinh has a natural area of approximately 5959.38 km², bounded by Nghe An province to the north, Quang Binh province to the south, the Lao People's Democratic Republic to the west, and the East Sea to the east. The population is about 1.3 million people, with livelihoods mainly depending on agriculture, forestry, aquaculture, and small-scale industries.

The topography of Ha Tinh is highly diverse, ranging from mountainous areas in the west to low-lying plains and coastal zones in the east (Le et al., 2021). The region is characterized by a dense river network, with major rivers such as the La river, Ngan Sau river, and Ngan Pho river flowing into the East Sea. This complex terrain, combined with the monsoon climate and high annual rainfall (averaging over 2,000 mm), makes Ha Tinh particularly vulnerable to flooding and water-related disasters (Loi et al., 2022). In addition, rapid socio-economic development, including the expansion of industrial zones, national roads, and the Vung Ang deep-sea port, has increased pressure on land use and further influenced flood susceptibility patterns. Overall, Ha Tinh provides a representative case study for flood risk assessment in Vietnam's central provinces, where natural conditions and human activities interact to create high exposure to flood hazards.

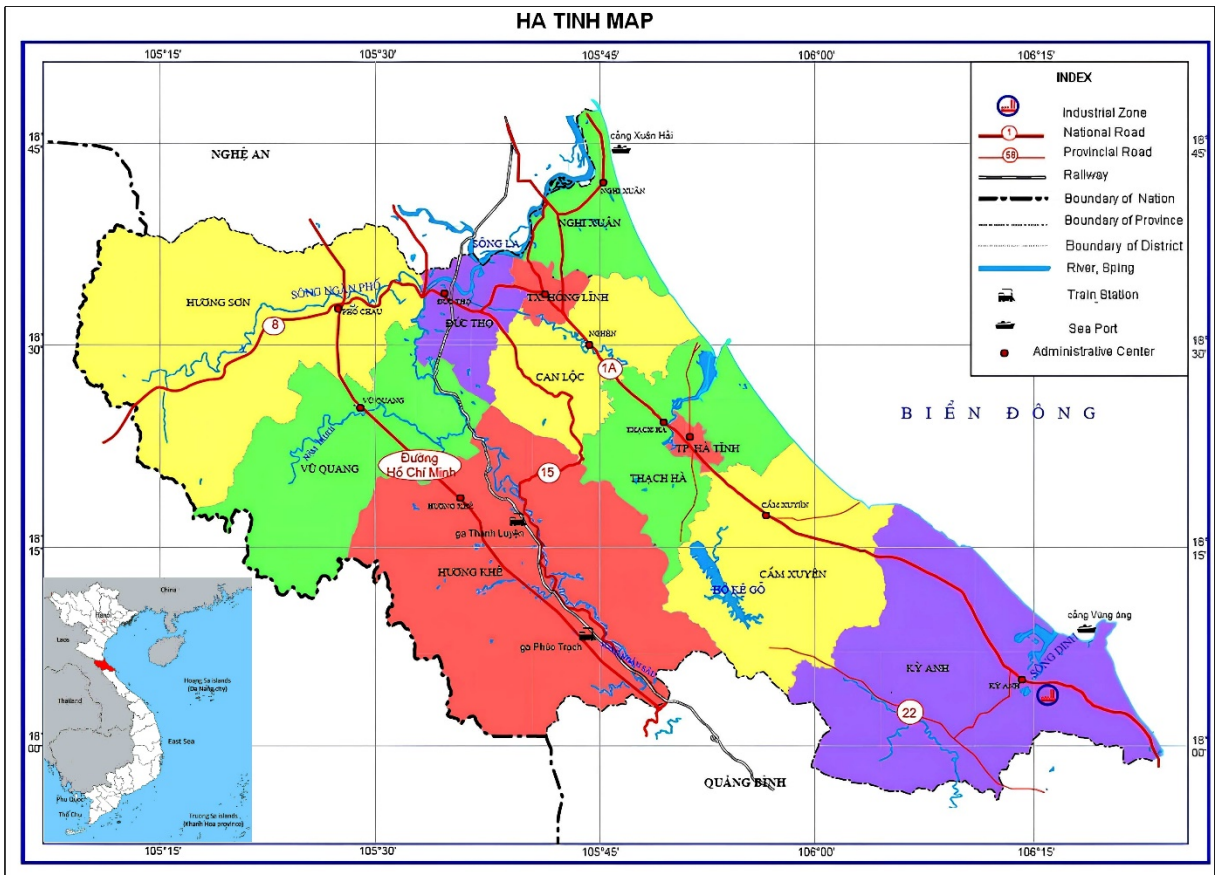

Figure 1. Location of the study area

2.2. Data sources

This study employed a combination of remote sensing products and ancillary datasets to derive the indicators used for flood risk assessment. Six primary data sources were collected, each corresponding to one of the selected indicators:

- Hydrological data: The river network is taken from the Ministry of Natural Resources and Environment data source, providing vector river layers used to generate distance rasters from near to the river.

- Topographic data: Elevation, slope and orientation were extracted from the database of the Ministry of Natural Resources and Environment with a spatial resolution of 30 m, ensuring full representation of terrain features.

- Land use/land cover (LULC): Land cover information was obtained from a Sentinel-2 satellite image land cover classification map collected on April 2, 2025, providing detailed land cover classes across the study area.

- Precipitation: Annual rainfall data were acquired from the Climate Hazards Group InfraRed Precipitation with Stations (CHIRPS) dataset at a ~5 km spatial resolution (Funk et al., 2015). The year 2025 was selected as a representative baseline observation period to capture the spatial distribution of recent intense monsoonal rainfall that coincided with major regional hydro-meteorological events and synchronized with the temporal acquisition of the Sentinel-2 land cover classification.

- Administrative boundary: Vector boundary of Ha Tinh province is taken from the database of the Ministry of Natural Resources and Environment for convenient cutting and displaying results.

- Infrastructure data: Land use planning maps were collected from the Department of Natural Resources and Environment for contextual analysis.

All datasets were projected to a common coordinate system (EPSG:4326) and resampled to consistent spatial resolution prior to analysis. The integration of multi-source datasets from global repositories and national agencies ensured both spatial detail and thematic accuracy for constructing flood risk indicators.

2.3. Methodology

The research process is designed to combine the Analytic Hierarchy Process (AHP) method with machine learning algorithms to build a flood risk map systematically and objectively. The entire data processing steps are shown in Figure 2, including the following main stages:

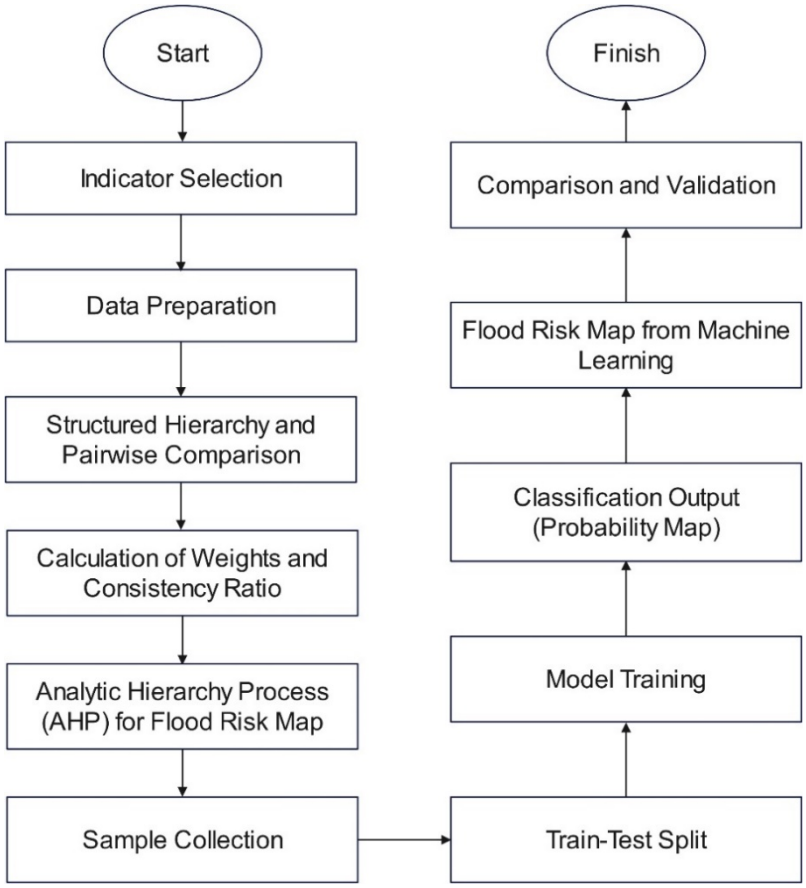

Figure 2. Flowchart of data processing in this study

2.3.1. Indicator selection

In the development of a flood risk map, the initial and fundamental step is the selection of indicators that can effectively represent the key factors influencing flood hazards. This selection is based on theoretical foundations regarding the impacts of natural, anthropogenic, and hydro-meteorological conditions on flood occurrence, supported by previous research findings and the availability of reliable datasets (Kılıç & Bektaş Balçık, 2025). Six major indicators were identified for this study:

(i) proximity to stream, which reflects the higher flood susceptibility of areas located close to river networks;

(ii) slope, a crucial factor determining surface runoff velocity and water accumulation capacity;

(iii) elevation, which indicates the vulnerability of low-lying areas to inundation compared to flood water levels;

(iv) aspect, related to wind direction and rainfall distribution, thereby indirectly affecting surface flow concentration;

(v) land use/land cover (LULC), which distinguishes differences in infiltration and water retention capacity across land cover types, influencing flood dynamics;

(vi) annual precipitation of 2025, a direct meteorological driver captured to reflect specific seasonal baseline intensity during the baseline observation year.

The integration of these indicators ensures a comprehensive assessment, simultaneously capturing the natural baseline conditions and human environment interactions, thereby providing a robust scientific foundation for subsequent analytical steps in flood risk evaluation.

2.3.2. Data preparation

In this step, all selected indicators are collected, standardized, and prepared for analysis. Proximity to stream is constructed by rasterizing the river network and calculating the Euclidean distance to the nearest river. Slope, elevation, and aspect are obtained from the MONRE database, land use/land cover is constructed using the classification of Sentinel-2 remote sensing imagery collected on April 2, 2025 using the Random Forest algorithm, and annual rainfall is compiled from CHIRPS daily rainfall in 2025. All datasets are clipped to the study area, projected to EPSG:4326, and resampled to a common spatial resolution (10 m).

To make indicators comparable, values are normalized using the min max method (Mazziotta & Pareto, 2022):

$$X' = \frac{X - X_{min}}{X_{max} - X_{min}} \quad (1)$$

where X' is the normalized value, ranging from 0 to 1. This procedure removes unit differences (for example, slope in degrees, elevation in meters, precipitation in millimeters) and ensures equal contribution of each factor. The processed and normalized layers are then exported and validated, forming a consistent dataset for subsequent AHP analysis.

2.3.3. Structured hierarchy and pairwise comparison

In this step, the selected indicators are organized into a hierarchical structure that reflects the overall objective, the evaluation criteria, and their respective sub-factors. At the top level, the objective is to assess flood risk, while the second level consists of the six chosen indicators: proximity to stream, slope, elevation, aspect, land use/land cover, and precipitation. The Analytic Hierarchy Process (AHP) is then applied to quantify the relative importance of each indicator through pairwise comparisons.

The pairwise comparison matrix utilized in this study was constructed through a structured expert consultation process involving a multidisciplinary panel of five independent specialists in Vietnam: two hydrologists specializing in river basin dynamics, two GIS and remote sensing

analysts with extensive regional mapping experience, and one disaster risk management officer familiar with local flooding conditions in Central Vietnam. The consultation followed a two-round Delphi-based consensus procedure. In the first round, each expert independently evaluated the relative importance of the six conditioning factors on Saaty's 1–9 fundamental scale. In the second round, divergent scores were shared anonymously, discussed, and iteratively adjusted to achieve a consolidated consensus judgment. In the pairwise comparison method, experts or prior studies are used to assign preference values on a scale from 1 to 9, where 1 denotes equal importance and 9 denotes extreme preference of one factor over another. These judgments form a pairwise comparison matrix $A = [a_{ij}]$, in which each element a_{ij} represents the importance of indicator i compared to indicator j, and the reciprocal property $a_{ij} = 1/a_{ji}$ holds (Kwiesielewicz & Van Uden, 2004).

From this matrix, the normalized principal eigenvector provides the weights of the indicators (Sabzi & King, 2015):

$$w_i = \frac{\lambda_i}{\sum_{j=1}^{n} \lambda_j} \tag{2}$$

where w_i is the weight of indicator i and λ_i is the eigenvalue associated with the comparison matrix. To verify the consistency of expert judgments, the Consistency Index (CI) and Consistency Ratio (CR) are calculated (Aguarón & Moreno-Jiménez, 2003):

$$CI = \frac{\lambda_{max}}{n-1} \tag{3}$$

$$CR = \frac{CI}{RI} \tag{4}$$

where λ_{max} is the maximum eigenvalue of the matrix, n is the number of indicators, and RI is the Random Index based on matrix size. A CR value less than 0.1 indicates acceptable consistency (Sato & Tan, 2023). Through this process, the relative weights of the indicators are determined in a systematic and logical manner, ensuring that the subsequent flood risk index reflects both expert knowledge and a mathematically consistent framework.

2.3.4. Calculation of weights

Based on the results of the pairwise comparison matrix and the eigenvector method, the relative weights of the six indicators were derived. These weights represent the degree of influence each factor has on flood risk within the study area. The calculation ensures that all weights sum to 1, thereby enabling a weighted linear combination of the normalized indicators. In this study, the final weights obtained were as follows: proximity to stream (0.523), slope (0.193), land use/land cover (0.152), elevation (0.054), aspect (0.037), and precipitation (0.040) (Table 1).

These values indicate that proximity to stream is the most influential factor, reflecting the high vulnerability of areas located near major waterways. Slope and land use/land cover follow as important determinants, capturing the role of surface runoff dynamics and human modifications of the landscape. By contrast, elevation, aspect, and precipitation contribute less but remain essential in providing a comprehensive assessment of flood susceptibility ((Kılıç & Bektaş Balçık, 2025). These weights serve as critical inputs for constructing the Flood Risk Index in the following step, ensuring that each indicator contributes proportionally to its relative importance.

Table 1. The weights of the indicators

Indicators	Proximity to stream	Slope	LULC	Elevation	Aspect	Annual Precipitation	Weight
Proximity to stream	1	5	6	7	7	9	0.524
Slope	1/5	1	2	5	5	5	0.193
LULC	1/6	1/2	1	5	5	5	0.152
Elevation	1/7	1/5	1/5	1	3	1	0.054
Aspect	1/7	1/5	1/5	1/3	1	1	0.037
Annual Precipitation	1/9	1/5	1/5	1	1	1	0.040
Sum of weights							1.000
CR	0.078						

2.3.5. AHP Flood Risk Index

Using the AHP-derived weights, the normalized indicator layers are combined into a single Flood Risk Index (FRI) via a weighted linear combination (WLC). Let $P, S, L, E, A, R \in [0,1]$ denote the min max normalized rasters of proximity to stream, slope, land use/land cover, elevation, aspect, and precipitation, respectively; and let the corresponding weights be $w_P = 0.524, w_S = 0.193, w_L = 0.152, w_E = 0.054, w_A = 0.037, w_R = 0.040$ (with $\sum w_i = 1$). The index is computed for each pixel as:

$$\text{FRI} = w_P P + w_S S + w_L L + w_E E + w_A A + w_R R \quad (5)$$

To aid interpretation and stabilize across scenes, the aggregated FRI can be re-normalized to [0,1] (Ghosh & Kar, 2018):

$$\text{FRI}' = \frac{\text{FRI} - min(\text{FRI})}{max(\text{FRI}) - min(\text{FRI})} \quad (6)$$

To facilitate spatial interpretation and territorial planning, the continuous Flood Risk Index ($\text{FRI}' \in [0,1]$) was categorized into five susceptibility classes using an Equal Interval classification scheme (Thammaboribal et al., 2025). The decision to employ the Equal Interval technique over statistical clustering methods (such as Natural Breaks) is methodologically deliberate. Because both the aggregated AHP index and the subsequent SVM probability outputs are strictly normalized across a uniform domain of [0,1], an equal-interval partitioning preserves the continuous linear and mathematical properties of the raw indicator scales. Statistical clustering algorithms inevitably introduce scene-dependent cut-offs that create artificial groupings and obscure direct spatial comparisons across different model outputs. In contrast, dividing the [0,1] range into five symmetrical 0.20 increments establishes an objective, transparent, and unbiased baseline, allowing seamless cross-comparison between the multi-criteria index and machine learning probability surfaces (Ghosh & Kar, 2018):

- Low Risk: $0.0 \leq \text{FRI}' < 0.2$

- Moderate Risk: $0.2 \leq \text{FRI}' < 0.4$

- Risky: $0.4 \leq FRI' < 0.6$

- High Risk: $0.6 \leq FRI' < 0.8$

- Very High Risk: $0.8 \leq FRI' \leq 1.0$

This step yields the AHP-based flood risk map, which serves both as a standalone product and as a basis for sampling/labeling in the subsequent machine-learning workflow.

2.3.6. Sample collection

In Ha Tinh province, historical flood records are traditionally documented in administrative text reports rather than being archived as structured geospatial data (such as vector points or polygons). These official reports primarily provide qualitative and descriptive statistics, including general administrative locations, broad inundation areas, and estimated flood depths, which lack the precise geographic coordinates required for spatial modeling. Consequently, directly obtaining pre-existing, georeferenced historical flood point datasets from local flood control departments for model training and validation is practically unfeasible.

Once the initial AHP flood hazard map was generated, representative sample points were collected to train and evaluate the SVM classifier. In this step, only the two extreme hazard categories: Low Risk (safe zone) and Very High Risk (hazardous zone), were selected to draw sample points, while the intermediate transitional classes (Moderate, Risky, and High) were intentionally excluded. The scientific rationale for this sampling strategy lies in maximizing feature-space contrast while minimizing boundary noise. In multi-criteria spatial evaluations, transitional zones often exhibit subtle parameter differences and substantial feature overlap, which can introduce ambiguity during supervised training. By focusing exclusively on contrasting terminal endpoints, the SVM algorithm can construct a more distinct and geometrically stable separating hyperplane in the kernel-transformed feature space. Once this optimal decision boundary is established, applying the trained model to the continuous feature stack effectively predicts the flood probabilities across the entire province, naturally interpolating the intermediate susceptibility gradients without being distorted by transitional noise (Wang et al., 2025).

Sampling was carried out using a stratified random approach, in which a predefined number of points were distributed proportionally across the selected risk classes. Specifically, 1000 points were drawn from the low risk class and another 1000 points from the very high risk class. Each sampled point inherited the spectral and thematic information from the six normalized indicators (proximity to stream, slope, land use, elevation, aspect, and precipitation) and was assigned a binary label: “0” for low risk areas and “1” for very high risk areas.

To avoid bias and overfitting, the combined dataset of 2000 samples was then randomly split into two subsets: 70% for training and 30% for testing. This division balances the need for sufficient training data with the requirement for independent evaluation (Zha et al., 2025). By leveraging the AHP-based map as a sampling guide, this step establishes a consistent and scientifically grounded training dataset, ensuring that the subsequent machine learning models are both well-informed and objectively validated.

2.3.7. Feature stack

After collecting and labeling the training and validation samples, the next step is to construct the feature stack, which integrates all selected indicators into a single multi-band dataset. Each band in

this stack corresponds to one normalized indicator: proximity to stream, slope, land use/land cover, elevation, aspect, and precipitation. By combining these layers, each sample point or pixel is represented by a vector of six values, reflecting the multi-dimensional conditions that influence flood risk. In practice, this was achieved by concatenating the normalized raster layers into one composite image using Google Earth Engine. The resulting dataset ensures that every spatial location within the study area has consistent and co-registered values across all indicators. Normalization guarantees that the features are dimensionless and lie within the range [0,1], preventing disparities in scale from biasing the model (Singh & Singh, 2022). The feature stack is then used to extract values for the sample points obtained in Step 6. Each point thus forms a record in the training dataset, with six predictor variables (the indicators) and one response variable (the flood risk class). This structured dataset is essential for supervised machine learning, as it allows algorithms to learn patterns that link the multi-indicator conditions to observed flood susceptibility (Ireland et al., 2015).

2.3.8. Model training

After preparing the feature set and labeled samples, the next step is to train supervised machine learning models to predict the probability of flood occurrence. In this study, the Support Vector Machine (SVM) algorithm is used. SVM is widely used in geospatial classification tasks (Hashim et al., 2021). For SVM, the Radial Basis Function (RBF) kernel was adopted to handle the nonlinear relationships between predictors and flood risk classes. The kernel function is expressed as (Tehrany et al., 2015; Pham et al., 2020):

$$K(x_i, x_j) = exp\left(-\gamma \|x_i - x_j\|^2\right) \quad (7)$$

where x_i and x_j are feature vectors, and γ is the kernel parameter controlling the influence of a single training sample. The cost parameter C balances the trade-off between maximizing the margin and minimizing classification error. In this study, γ = 0.1 and C = 100 were selected after preliminary testing. The model outputs class probabilities, which provide a continuous measure of flood risk. The training dataset (70% of samples) was used to fit the models, while the remaining 30% served as an independent test set. Both classifiers were set to output probability surfaces, which were later converted into susceptibility classes. This step enables the machine learning models to generalize from the labeled samples and generate spatially continuous flood risk maps across the study area (Antzoulatos et al., 2022).

2.3.9. Classification output

After training the machine learning models, the next step is to generate spatially continuous flood susceptibility maps by applying the trained classifiers to the entire feature stack. In the SVM model, the RBF kernel outputs a probability value between 0 and 1, representing the likelihood of flood risk at each location.

To make the results more interpretable, these continuous probability surfaces are transformed into discrete susceptibility classes. A five-level classification scheme was adopted, with thresholds defined as follows (Thammaboribal et al., 2025):

- Low Risk: $0.0 \leq P < 0.2$

- Moderate Risk: $0.2 \leq P < 0.4$

- Risky: $0.4 \leq P < 0.6$

- High Risk: $0.6 \leq P < 0.8$

- Very High Risk: $0.8 \leq P \leq 1.0$

where P is the model-derived probability of flood risk. This classification approach ensures consistency with the AHP-based flood risk map. The classified output is visualized using a color palette ranging from green (low risk) to red (very high risk), which highlights spatial patterns of vulnerability across the study area. The raster maps are also exported in a standard coordinate system (EPSG:4326) for further analysis, reporting, and integration into Geographic Information Systems (GIS). By converting probabilistic outputs into susceptibility categories, this step bridges the gap between statistical modeling and practical decision-making, providing stakeholders with actionable spatial information on flood hazards.

2.3.10. Comparison and validation

The final step of the methodology is to compare and validate the results obtained from the AHP-based method combined with the machine learning model. This ensures that the generated flood risk maps are both reliable and scientifically sound. The validation is performed using an independent test dataset (30% of the total sample) that was not included in the training phase. For each validation point, the predicted class values were extracted from the flood risk map obtained by machine learning and compared with the corresponding AHP-derived class labels to calculate standard accuracy metrics. It should be emphasized that because the validation points originate from the expert-based zoning, the resulting Overall Accuracy (OA) and Kappa coefficient reflect internal spatial agreement and boundary-smoothing performance rather than absolute predictive accuracy against real-world flood footprints. Key performance indicators include overall accuracy (OA) and the Kappa index derived from the confusion matrix. In addition to statistical validation, spatial comparisons were also performed between the maps. The study overlaid flood risk maps with current status and planning maps of the province to assess the key areas of the province in detail. The combination of quantitative validation and spatial comparison provides a comprehensive assessment of the model performance, ensuring that the final flood risk mapping results are both accurate and useful in practice.

3. Results and discussion

Figures 3 to 8 sequentially present the thematic maps used for flood risk analysis in the study area, including the land use/land cover map for 2025 (Fig. 3), the proximity to stream map (Fig. 4), the annual precipitation map (Fig. 5), the slope map (Fig. 6), the aspect map (Fig. 7), and the elevation map (Fig. 8). These maps provide essential datasets for constructing the flood risk index based on the AHP method and for integration with the machine learning model. The area and percentage share of the respective flood risk levels in the study area are presented in Table 2.

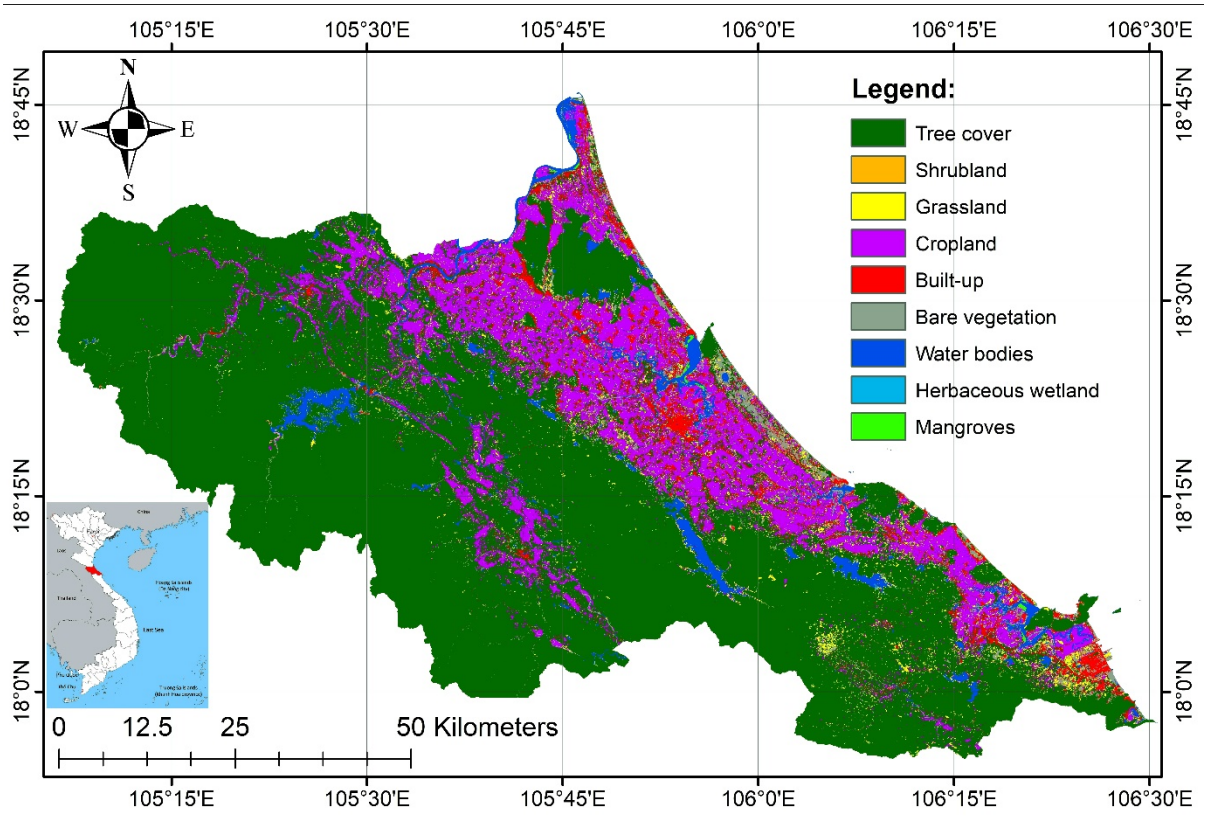

Figure 3. Land use/cover map of the study area

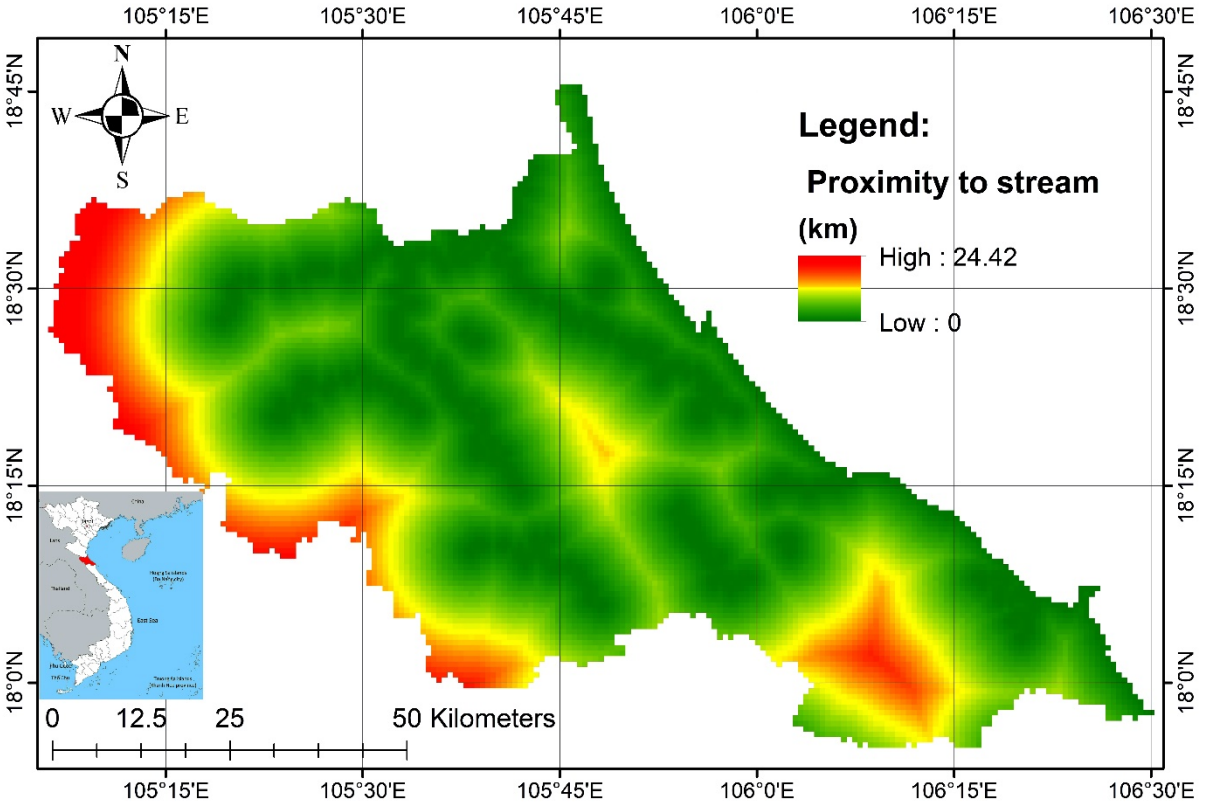

Figure 4. Proximity to stream map of the study area

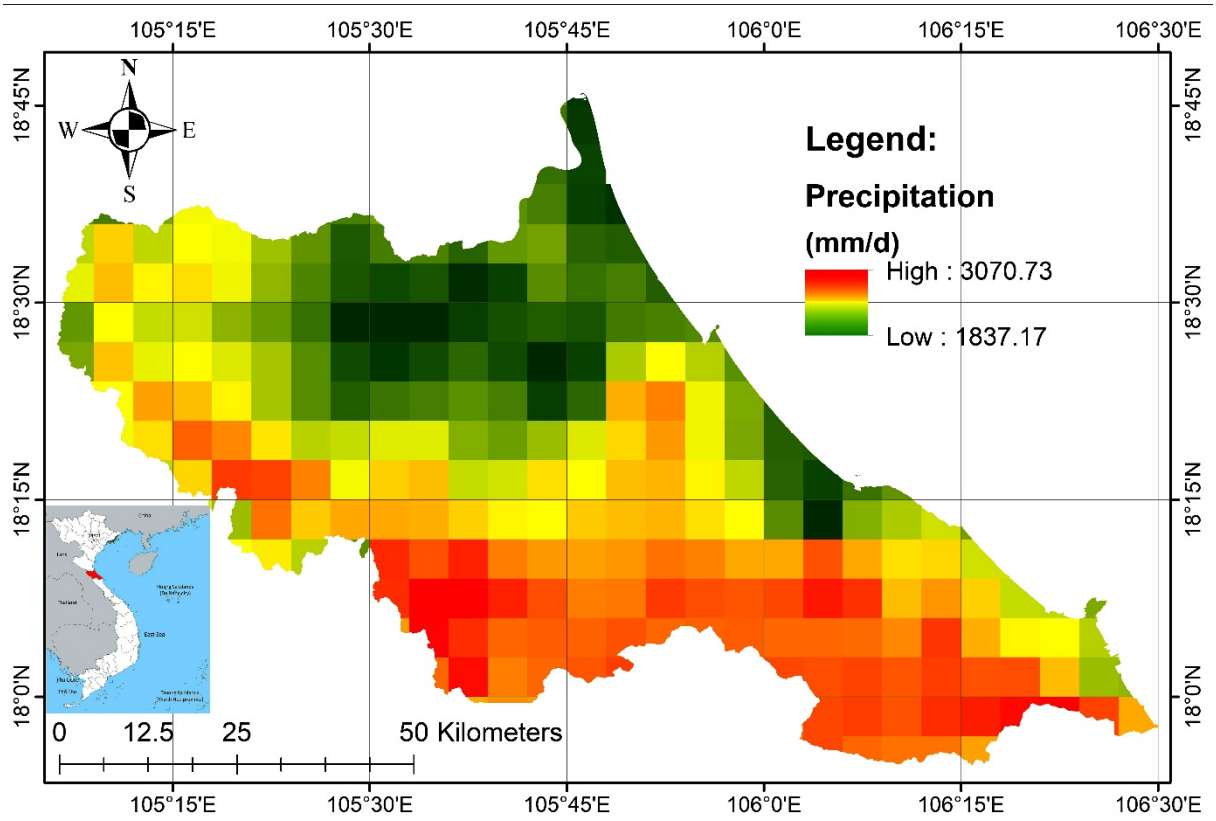

Figure 5. Precipitation map of the study area

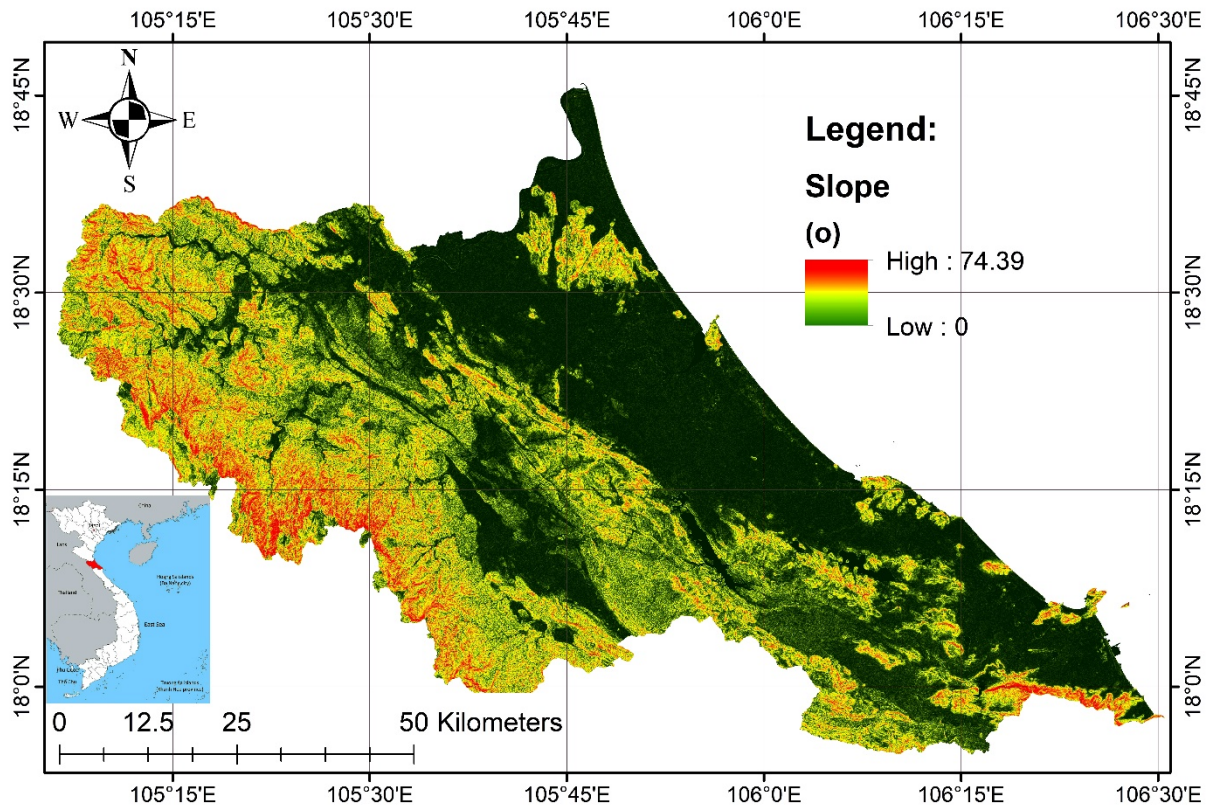

Figure 6. Slope map of the study area

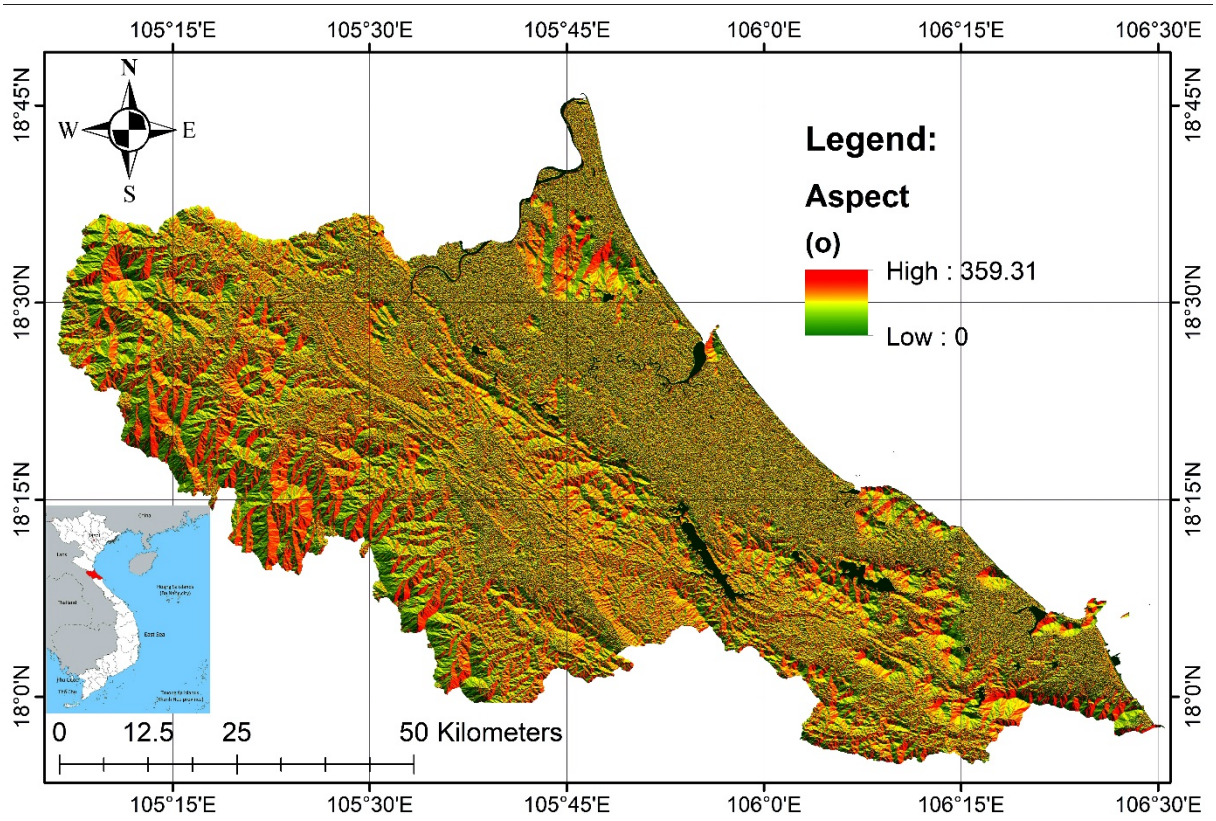

Figure 7. Aspect map of the study area

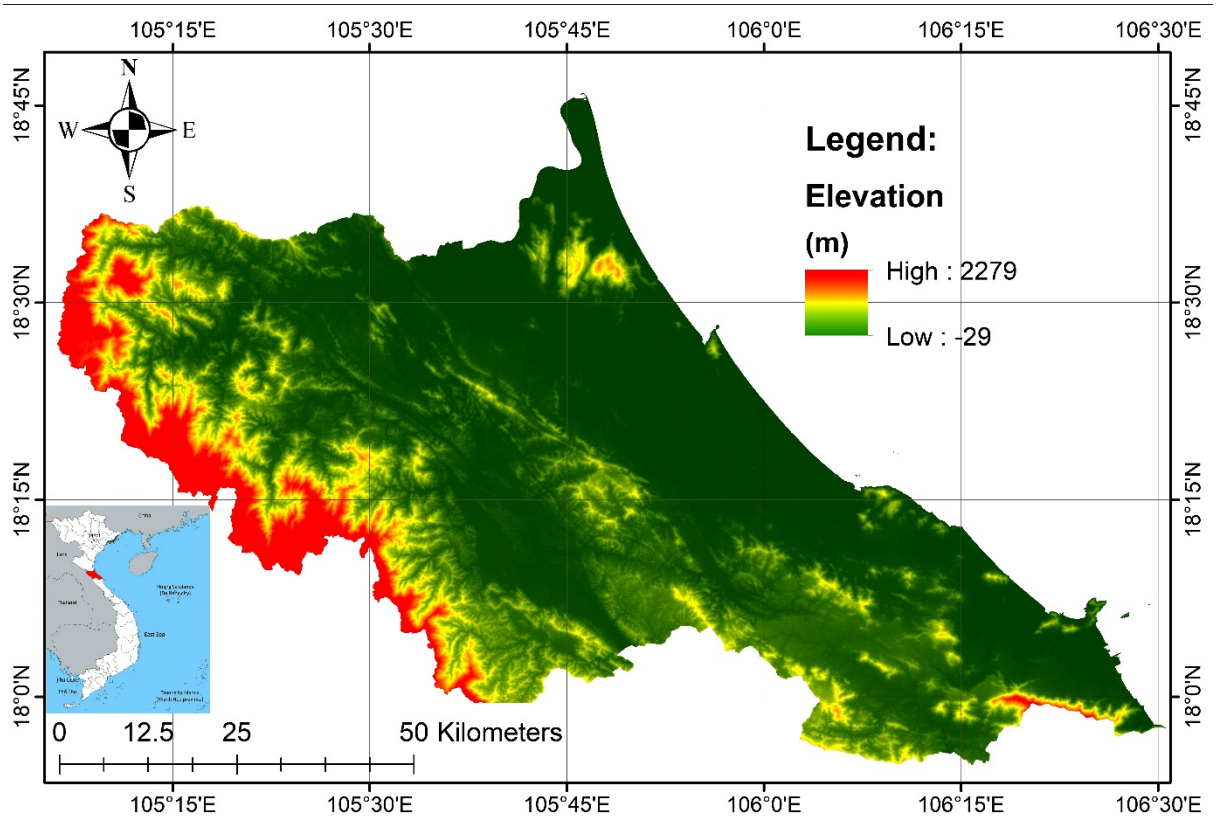

Figure 8. Elevation map of the study area

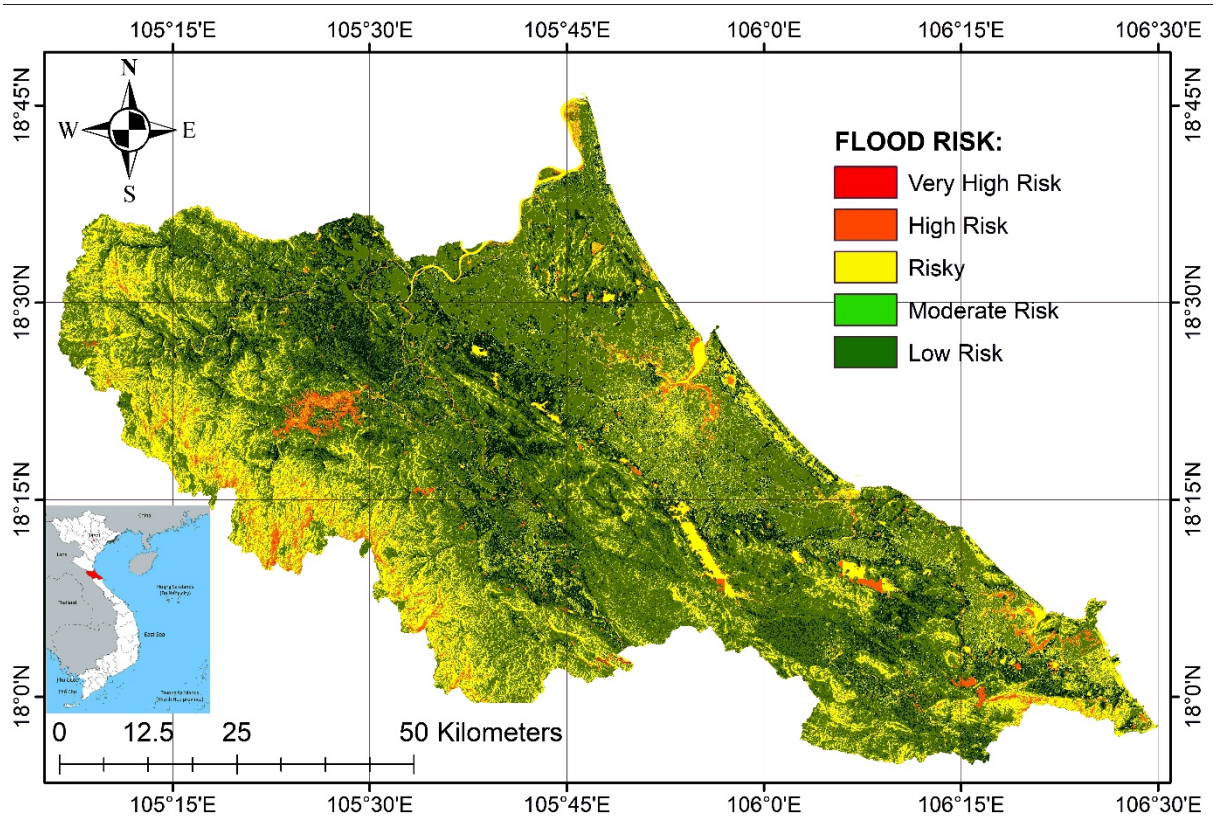

Figure 9. Flood risk map from AHP of the study area

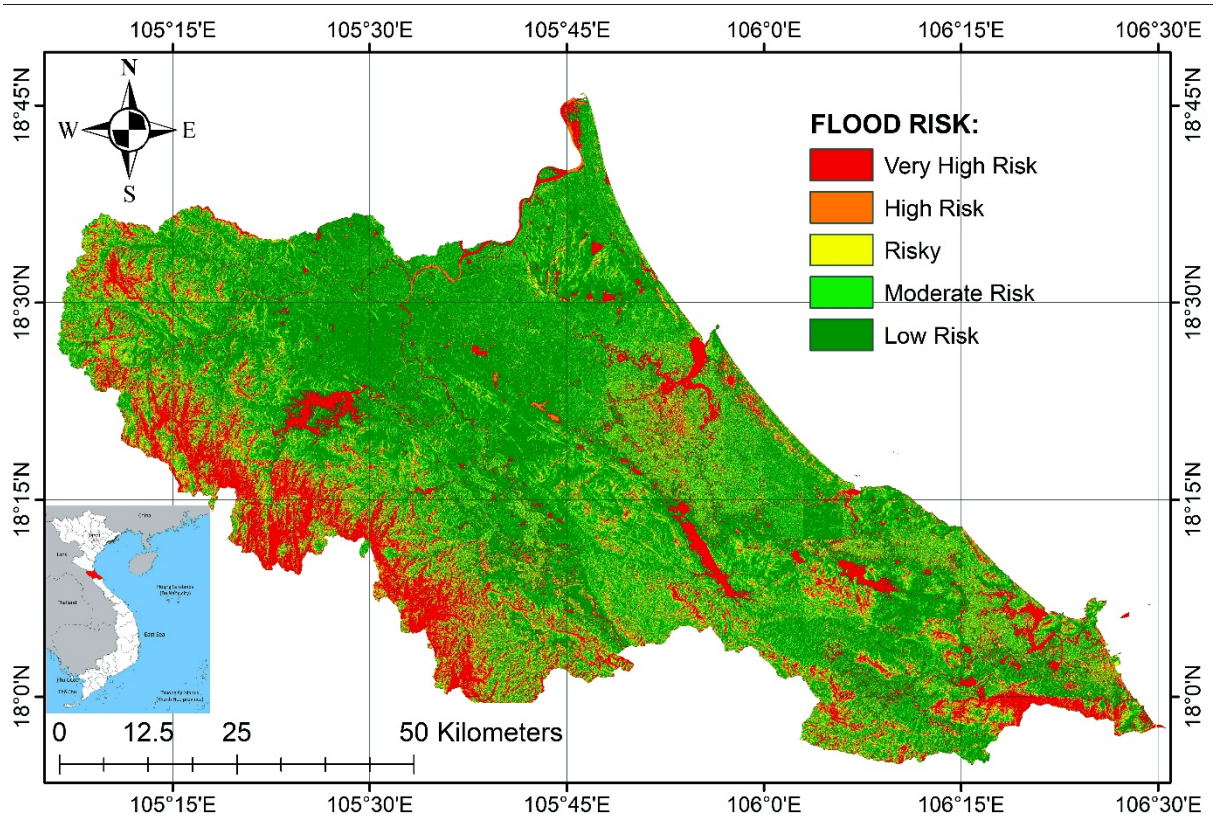

Figure 10. Flood risk map from AHP combine with machine learning of the study area

Figure 10 illustrates the flood hazard zonation generated by the integrated AHP-SVM workflow. A critical physical pattern is the prominent "very high risk" belt concentrated along the

western and south-western highland sectors of the province. Rather than an artifact of subjective weighting, this spatial clustering is driven by compounding hydro-geomorphic mechanics:

1. Topographic triggers: The western flank of Ha Tinh features steep mountain ranges with local slope gradients exceeding 70° (Fig. 6) and elevations up to 2,279 m (Fig. 8), which sharply reduce rainfall infiltration and drastically compress hydrological concentration times.

2. Orographic enhancement: These elevated ranges from an impermeable topographic barrier to seasonal monsoonal air masses moving inland from the East Sea, forcing intense orographic lifting and generating concentrated annual rainfall surpassing 3,000 mm/year (Fig. 5).

3. Channel hydraulics: Runoff generated by this intense orographic precipitation discharges directly into the steep, deeply incised, and structurally confined headwater catchments of the Ngan Sau and Ngan Pho river networks. The narrow valleys rapidly funnel torrential discharge downstream, inducing extreme flow velocities and substantial hydrodynamic pressures. These compounding factors explain why the western corridor is naturally predisposed to severe flash floods and associated hillslope debris flows.

Table 2. Area and percentage of flood risk levels in the study area

Level	Area (km^2)	Percentage (%)
Low risk	833.72	13.99
Moderate risk	585.21	9.82
Risky	672.81	11.29
High risk	1027.40	17.24
Very high risk	2840.24	47.66

Table 2a. Quantitative comparison of flood risk areas between the standalone AHP and integrated AHP-SVM models

Flood Risk Level	Standalone AHP Area (km^2)	Standalone AHP (%)	Integrated AHP-SVM Area (km^2)	Integrated AHP-SVM (%)	Area Difference (km^2)
Low risk	914.11	15.34%	833.72	13.99%	-80.39
Moderate risk	3340.64	56.06%	585.21	9.82%	-2755.43
Risky	1492.12	25.04%	672.81	11.29%	-819.31
High risk	206.94	3.47%	1027.40	17.24%	820.46
Very high risk	5.57	0.09%	2840.24	47.66%	2834.67

A quantitative cross-comparison between the standalone AHP map (Fig. 9) and the integrated AHP-SVM map (Fig. 10) confirms a distinct redistribution of hazard classifications (Table 2a). Under the standalone AHP model, hazard distributions are substantially skewed toward

the lower susceptibility tiers: 71.40% of the provincial territory (4,254.75 km²) is categorized as Low Risk (15.34%) or Moderate Risk (56.06%), whereas the High Risk and Very High Risk zones account for merely 3.47% (206.94 km²) and 0.09% (5.57 km²), respectively. This conservative skewness stems from the inherent nature of weighted linear combination (WLC), in which the averaging of normalized indicator scores attenuates extreme spatial values and causes widespread pixel-level fragmentation.

Conversely, the integrated AHP-SVM framework substantially expands the contiguous high-exposure footprint: the High Risk category increases to 1,027.40 km² (+820.46 km²), and the Very High Risk category reaches 2,840.24 km² (+2,834.67 km²). By projecting multi-source conditioning factors into a non-linear feature space via the RBF kernel, the SVM classifier effectively resolves the step-like boundary artifacts of linear indexing. Consequently, transitional and low-lying drainage channels that were previously fragmented under AHP are reconstructed into hydrologically cohesive flow corridors and continuous hazard belts (Fig. 10). This continuity provides an operationally viable hazard baseline for spatial planning evaluations, eliminating the localized noise of standalone index overlays.

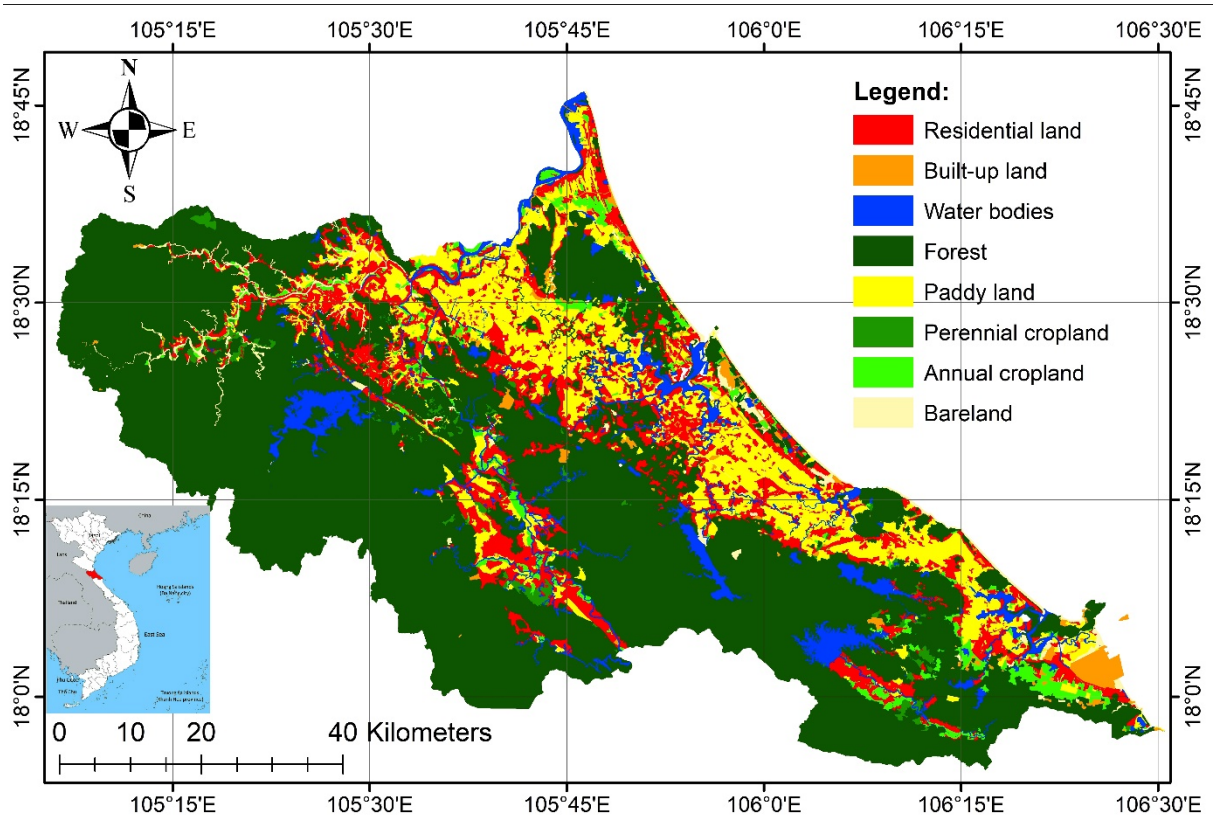

Figure 11. Land use planning map of Ha Tinh province in 2030

To assess the level of compatibility between flood risk and future land use orientation, the study overlaid the flood risk zoning map with the land use planning map in 2030. Figure 11 shows the land use planning map of Ha Tinh province in 2030.

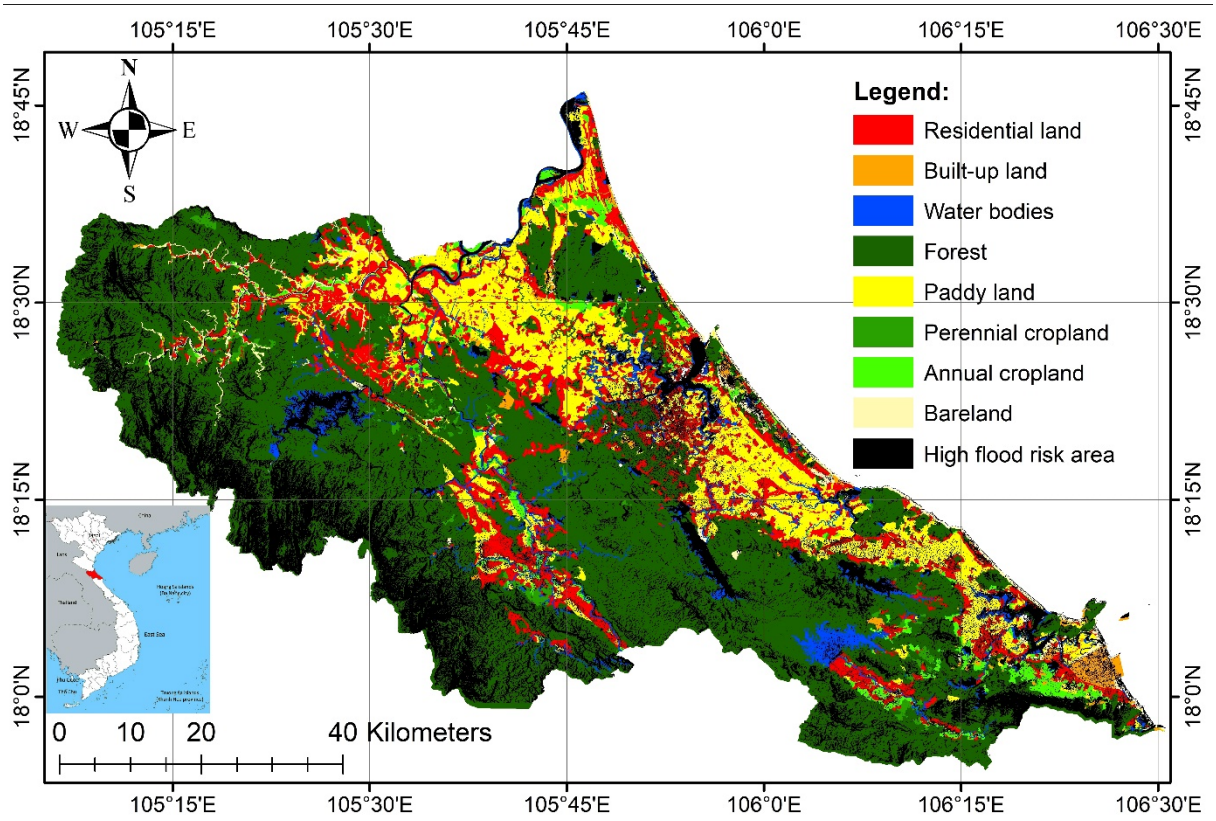

Figure 12. Spatial overlap between the 2030 land use planning and high flood risk zones in Ha Tinh province

The overlay results reveal that areas of very high flood risk are concentrated primarily in the western forested and mountainous zones, particularly in upstream valleys along rivers and streams, where steep terrain, orographic rainfall, and limited infiltration capacity accelerate surface runoff, leading to flash floods, landslides, and rapid inundation (Fig. 12). Settlements, transportation corridors, and agroforestry activities interspersed within these valleys are therefore exposed to extremely high risks. In the downstream plains and coastal lowlands, flood hazards range from moderate to high, concentrated along major rivers and densely populated/urbanized areas, resulting in deep and prolonged inundation. Overall, Ha Tinh's flood risk structure consists of a belt of very high risk in the western highlands (flash floods and landslides) and a zone of medium to high risk in the downstream lowlands (riverine flooding), implying the necessity to strictly control land use along forested valleys, prioritize flood drainage infrastructure, and adopt adaptive settlement planning in the 2030 land-use framework.

Table 3. The area of land use classes according to the 2030 land use planning map of Ha Tinh province located in high flood risk zones

Class	Residential land	Built-up land	Water bodies	Forest	Paddy land	Perennial cropland	Annual cropland	Bareland
Area (km^2)	613.77	55.71	138.24	2412.12	622.83	63.87	164.03	30.08
Total	4,100.65 km^2							

Table 3 indicates that the area of land use classes under the 2030 land use planning map of Ha Tinh Province located in high flood risk zones amounts to 4,100.65 km², accounting for a substantial proportion of the province's total natural area. Among them, forest is the most affected with more than 2412.12 km², reflecting that flood hazards are not only concentrated in the coastal plains but also extend into the western mountainous regions, where flash floods and landslides are likely to occur. Paddy land (622.83 km²) and residential land (613.77 km²) also occupy significant proportions, highlighting the serious risks to food security and socio-economic infrastructure if planning is implemented without adaptive measures. Other land types, such as annual cropland (164.03 km²), water bodies (138.24 km²), perennial cropland (63.87 km²), built-up land (55.71 km²), and bare land (30.08 km²), although less affected in area, still require attention as they are associated with essential production activities, services, and livelihoods. Overall, the analysis confirms that high flood risk affects almost all land use classes in the 2030 planning framework, posing major challenges for spatial socio-economic development and emphasizing the necessity of integrating disaster risk and climate change considerations into land use planning and management.

While the integrated AHP-SVM framework demonstrates clear operational advantages in smoothing linear decision boundaries and establishing hydrologically cohesive hazard zones, several methodological limitations warrant discussion. Foremost among these is the self-referencing nature of the training and evaluation workflow. Owing to the absence of systematically georeferenced historical flood archives in Ha Tinh province, both training and testing datasets were drawn directly from the initial AHP classification. Consequently, the high statistical agreement achieved by the model—reflected in an Overall Accuracy of 92.5% and a Kappa coefficient of 0.85—quantifies internal mathematical consistency and spatial boundary fidelity rather than empirical predictive accuracy against ground-truth inundation scars. Furthermore, relying on CHIRPS precipitation data from a single baseline year (2025) imposes temporal constraints. While this setup effectively captures contemporary spatial rainfall patterns aligned with our satellite land-cover observations, it fails to encompass multi-decadal climatic anomalies, inter-annual precipitation dynamics, or extreme precipitation events with defined recurrence intervals. Additionally, the regional 30 m DEM cannot capture micro-topographic variations, engineered flood dikes, or localized urban drainage networks that strongly govern fine-scale hydraulic velocity and inundation depth.

To address these constraints, future investigations should advance the methodology along three complementary directions. First, decoupling the machine learning calibration from expert-based indices is essential; this can be achieved by processing multi-temporal Sentinel-1 SAR and Sentinel-2 optical imagery acquired during actual flood crises to construct an independent, empirical flood inventory. Second, bridging these continuous spatial susceptibility surfaces with dynamic 1D/2D hydrodynamic models, such as HEC-RAS or TELEMAC, will enable the numerical simulation of flow velocity, water depth, and recession time under changing climate scenarios. Finally, integrating fine-resolution elevation models derived from airborne LiDAR or drone photogrammetry will be critical to resolving local hydraulic barriers and supporting asset-level infrastructure protection within statutory territorial plans.

4. Conclusion

This study established an integrated spatial framework that couples multi-criteria decision analysis (AHP) with a Support Vector Machine (SVM) algorithm to assess regional flood hazard susceptibility and evaluate its structural compatibility with statutory territorial planning in Ha Tinh province, Vietnam. Rather than functioning as an empirical real-time forecasting tool, the primary methodological value of this workflow lies in its capability as a self-referencing spatial optimization instrument. By projecting multi-dimensional environmental indicators into a non-linear feature space via the RBF kernel, the model effectively eliminates the rigid, step-like fragmentation typical of linear index overlay, generating hydrologically cohesive and continuous hazard corridors across complex terrain gradients.

The spatial overlay reveals substantial exposure conflicts across future development zones, indicating that high-hazard belts heavily intersect planned forest lands, agricultural paddy fields, and newly designated residential expansion areas. These spatial misalignments emphasize that current territorial allocation strategies remain acutely vulnerable to hydro-meteorological extremes. Consequently, provincial authorities must urgently integrate non-structural risk zoning into statutory master planning. Strategic priorities should include enforcing strict land-use development moratoria along steep upstream corridors, establishing mandatory retention buffers around natural drainage paths, and implementing flood-resilient building standards in low-lying residential expansions. Moving forward, incorporating dynamic hydrodynamic simulations and empirical satellite-derived flood footprints will further decouple model calibration from expert assumptions, advancing resilient territorial governance under compounding climate challenges.

References

Aguarón, J., & Moreno-Jiménez, J. M. (2003). The geometric consistency index: Approximated thresholds. European journal of operational research, 147(1), 137-145.

Al-Kindi, K. M., & Alabri, Z. (2024). Investigating the role of the key conditioning factors in flood susceptibility mapping through machine learning approaches. Earth Systems and Environment, 8(1), 63-81. https://doi.org/10.1007/s41748-023-00369-7.

Amatebelle, C. E., Owolabi, S. T., Ogundeji, A. A., & Okolie, C. C. (2025). A systematic analysis of remote sensing and geographic information system applications for flood disaster risk management. Journal of Spatial Science, 1-27. https://doi.org/10.1080/14498596.2025.2476973.

Antzoulatos, G., Kouloglou, I.-O., Bakratsas, M., Moumtzidou, A., Gialampoukidis, I., Karakostas, A., Lombardo, F., Fiorin, R., Norbiato, D., Ferri, M., Symeonidis, A., Vrochidis, S., & Kompatsiaris, I. (2022). Flood Hazard and Risk Mapping by Applying an Explainable Machine Learning Framework Using Satellite Imagery and GIS Data. Sustainability, 14(6), 3251. https://doi.org/10.3390/su14063251.

Bojer, A. K., Abshare, M. W., Mesfin, F., & Al-Quraishi, A. M. F. (2025). Assessing climate and land use impacts on surface water yield using remote sensing and machine learning. Scientific Reports, 15(1), 18477. https://doi.org/10.1038/s41598-025-03493-8.

Dano Umar, L., Matori, A. N., Hashim, A. M., Chandio, I. A., Sabri, S., Balogun, A. L., & Abba, H. A. (2011). Geographic information system and remote sensing applications in flood hazards

management: A review. Research Journal of Applied Sciences, Engineering and Technology, 3(9), 933-947.

Donn-Arnold, N., Xaza, A. & Kanyerere, T. (2026). Smart Metering and Socio-Economic Approaches for Urban Water Sustainability during Drought in Cape Town, South Africa. Trends in Ecological and Indoor Environmental Engineering, 4(2), 72–84. https://doi.org/10.62622/TEIEE.026.4.2.72-84.

Dobrovičová, S., Dobrovič, R., & Dobrovič, J. (2015). The economic impact of floods and their importance in different regions of the world with emphasis on Europe. Procedia Economics and Finance, 34, 649–655. https://doi.org/10.1016/S2212-5671(15)01681-0.

Funk, Chris, Pete Peterson, Martin Landsfeld, Diego Pedreros, James Verdin, Shraddhanand Shukla, Gregory Husak, James Rowland, Laura Harrison, Andrew Hoell & Joel Michaelsen. (2015). The climate hazards infrared precipitation with stations-a new environmental record for monitoring extremes. Scientific Data 2, 150066. Doi:10.1038/sdata.2015.66 2015.

Ghosh, A., & Kar, S. K. (2018). Application of analytical hierarchy process (AHP) for flood risk assessment: a case study in Malda district of West Bengal, India. Natural Hazards, 94(1), 349-368. https://doi.org/10.1007/s11069-018-3392-y.

Glago, F. J. (2021). Flood disaster hazards; causes, impacts and management: a state-of-the-art review. Natural hazards-impacts, adjustments and resilience. Doi: 10.5772/intechopen.95048.

Goodess, C. M. (2013). How is the frequency, location and severity of extreme events likely to change up to 2060? Environmental science & policy, 27, S4-S14. https://doi.org/10.1016/j.envsci.2012.04.001.

Goumghar, L., Fri, R., Hajaj, S., Taia, S., & El Mansouri, B. (2025). Integrating geospatial data and analytic hierarchy process for flood-prone zones mapping in the Upper Draa basin, Morocco. Ecological Engineering & Environmental Technology (EEET), 26(4). https://doi.org/10.12912/27197050/201160.

Gu, X., Zhang, Q., Li, J., Chen, D., Singh, V. P., Zhang, Y. & Yu, H. (2020). Impacts of anthropogenic warming and uneven regional socio-economic development on global river flood risk. Journal of Hydrology, 590, 125262. https://doi.org/10.1016/j.jhydrol.2020.125262.

Hashim, F., Dibs, H., & Jaber, H. S. (2021, July). Applying support vector machine algorithm on multispectral remotely sensed satellite image for geospatial analysis. In Journal of Physics: Conference Series (Vol. 1963, No. 1, p. 012110). IOP Publishing. Doi: 10.1088/1742-6596/1963/1/012110.

Hoang, T. V., Chou, T. Y., Nguyen, N. T., Fang, Y. M., Yeh, M. L., Nguyen, Q. H., & Nguyen, X. L. (2019). A Robust Early Warning System for Preventing Flash Floods in Mountainous Area in Vietnam. ISPRS International Journal of Geo-Information, 8(5), 228. https://doi.org/10.3390/ijgi8050228.

Ireland, G., Volpi, M., & Petropoulos, G. P. (2015). Examining the Capability of Supervised Machine Learning Classifiers in Extracting Flooded Areas from Landsat TM Imagery: A

Case Study from a Mediterranean Flood. Remote Sensing, 7(3), 3372-3399. https://doi.org/10.3390/rs70303372

Istomina, M. N., & Dobrovoski, S. G. (2016). Floods of the world: quantitative analysis of natural characteristics and parameters of social-economic damages. Water Resources, 43(3), 459-471. https://doi.org/10.1134/S0097807816030076.

Jonkman, S. N. (2005). Global perspectives on loss of human life caused by floods. Natural hazards, 34(2), 151-175. https://doi.org/10.1007/s11069-004-8891-3.

Kiptum, A., Mwangi, E., Otieno, G., Njogu, A., Kilavi, M., Mwai, Z., & Todd, M. C. (2025). Advancing operational flood forecasting, early warning and risk management with new emerging science: Gaps, opportunities and barriers in Kenya. Journal of flood risk management, 18(1), e12884. https://doi.org/10.1111/jfr3.12884.

Kirshen, P., Watson, C., Douglas, E., Gontz, A., Lee, J., & Tian, Y. (2008). Coastal flooding in the Northeastern United States due to climate change. Mitigation and Adaptation Strategies for Global Change, 13(5), 437-451. https://doi.org/10.1007/s11027-007-9130-5.

Kılıç, G., & Bektaş Balçık, F. (2025). Flood-Risk Map for Büyükçekmece District Based on Socioeconomic Factors. Environmental and Earth Sciences Proceedings, 32(1), 11. https://doi.org/10.3390/eesp2025032011.

Kundzewicz, Z. W., Kanae, S., Seneviratne, S. I., Handmer, J., Nicholls, N., Peduzzi, P., Sherstyukov, B. (2013). Flood risk and climate change: global and regional perspectives. Hydrological Sciences Journal, 59(1), 1-28. https://doi.org/10.1080/02626667.2013.857411.

Kwiesielewicz, M., & Van Uden, E. (2004). Inconsistent and contradictory judgements in pairwise comparison method in the AHP. Computers & Operations Research, 31(5), 713-719. https://doi.org/10.1016/S0305-0548(03)00022-4.

Le, T. T. A., Willems, P., & Nguyen, L. A. (2023). Flood Hazard Analysis under Current and Future Climate Conditions for Ha Tinh Province, Vietnam. PhD Thesis.

Le, T. T. A., Lan-Anh, N. T., Daskali, V., Verbist, B., Vu, K. C., Anh, T. N., & Willems, P. (2021). Urban flood hazard analysis in present and future climate after statistical downscaling: a case study in Ha Tinh city, Vietnam. Urban Water Journal, 18(4), 257-274. https://doi.org/10.1080/1573062X.2021.1877744.

Loi, D. T., Huong, L. V., Tuan, P. A., Hong Nhung, N. T., Quynh Huong, T. T., & Hoa Man, B. T. (2022). An Assessment of Agricultural Vulnerability in the Context of Global Climate Change: A Case Study in Ha Tinh Province, Vietnam. Sustainability, 14(3), 1282. https://doi.org/10.3390/su14031282.

Mazziotta, M., & Pareto, A. (2022). Normalization methods for spatio-temporal analysis of environmental performance: Revisiting the Min–Max method. Environmetrics, 33(5), e2730. https://doi.org/10.1002/env.2730.

Munier, N., & Hontoria, E. (2021). Uses and Limitations of the AHP Method: A Non-Mathematical and Rational Analysis. Springer International Publishing: Berlin/Heidelberg, Germany. https://doi.org/10.1007/978-3-030-60392-2

Millimono, T. S. (2026). Risk Production and Urban Vulnerability in Conakry: Integrating Governance, Land Use, and Biophysical Factors in the 2025 Manéah Landslide. Trends in Ecological and Indoor Environmental Engineering, 4(2), 44–59. https://doi.org/10.62622/TEIEE.026.4.2.44-59

Nguyen, H. D. (2023). Spatial modeling of flood hazard using machine learning and GIS in Ha Tinh province, Vietnam. Journal of Water and Climate Change, 14(1), 200-222. doi: 10.2166/wcc.2022.257.

Nguyen, L. D., Nguyen, H. T., Dang, P. D., Duong, T. Q., & Nguyen, L. K. (2021). Design of an automatic hydro-meteorological observation network for a real-time flood warning system: a case study of Vu Gia-Thu Bon river basin, Vietnam. Journal of Hydroinformatics, 23(2), 324-339. https://doi.org/10.2166/hydro.2021.124.

Nguyen, D. L., Chou, T. Y., Hoang, T. V., & Chen, M. H. (2023). Flood susceptibility mapping using machine learning algorithms: a case study in Huong Khe District, Ha Tinh Province, Vietnam. International Journal of Geoinformatics, 19(7), 1-15.

Ortiz-Vargas, A.; Sebesvari, Z. (2021). Technical Report: Floods in Central Viet Nam. In Interconnected Disaster Risks 2020/2021; United Nations University-Institute for Environment and Human Security (UNU-EHS), Bonn, Germany.

Odiana, S., Godwin, O. G. & Okoduwa, A. K. (2026). Integrating Long-Term Climate Trend Analysis and Household Socioeconomic Vulnerability to Assess Climate Stress in the Niger Delta Floodplain (Ughelli, Nigeria). Trends in Ecological and Indoor Environmental Engineering, 4(2), 12–21. https://doi.org/10.62622/TEIEE.026.4.2.12-21.

Perera, D., Agnihotri, J., Seidou, O., & Djalante, R. (2020). Identifying societal challenges in flood early warning systems. International Journal of Disaster Risk Reduction, 51, 101794. https://doi.org/10.1016/j.ijdrr.2020.101794.

Pham, B. T., Phong, T. V., Nguyen, H. D., Qi, C., Al-Ansari, N., Amini, A., Ho, L. S., Tuyen, T. T., Yen, H. P. H., Ly, H.-B., Prakash, I., & Tien Bui, D. (2020). A Comparative Study of Kernel Logistic Regression, Radial Basis Function Classifier, Multinomial Naïve Bayes, and Logistic Model Tree for Flash Flood Susceptibility Mapping. Water, 12(1), 239. https://doi.org/10.3390/w12010239.

Pham, N. T. T., Nguyen, Q. H., Ngo, A. D., Le, H. T. T., & Nguyen, C. T. (2018). Investigating the impacts of typhoon-induced floods on the agriculture in the central region of Vietnam by using hydrological models and satellite data. Natural Hazards, 92(1), 189-204. https://doi.org/10.1007/s11069-018-3202-6.

Rajkhowa, S., & Sarma, J. (2021). Climate change and flood risk, global climate change. In: Global climate change, pp. 321-339. Elsevier. https://doi.org/10.1016/B978-0-12-822928-6.00012-5.

Ringo, J., Sabai, S., & Mahenge, A. (2025). Contribution of flood early warning response measures in reducing flood effects in Kilosa District, Tanzania. Climate Services, 37, 100534.

Sato, Y., & Tan, K. H. (2023). Inconsistency indices in pairwise comparisons: an improvement of the Consistency Index. Annals of Operations Research, 326(2), 809-830. https://doi.org/10.1007/s10479-021-04431-3.

Sabzi, H. Z., & King, J. P. (2015). Numerical comparison of multi-criteria decision-Making techniques: A simulation of flood management multi-criteria systems. In: World Environmental and Water Resources Congress 2015, pp. 359-373.

Singh, D., & Singh, B. (2022). Feature wise normalization: An effective way of normalizing data. Pattern Recognition, 122, 108307. https://doi.org/10.1016/j.patcog.2021.108307.

Singha, C., Chakraborty, N., Sahoo, S., Pham, Q. B., & Xuan, Y. (2025). A novel framework for flood susceptibility assessment using hybrid analytic hierarchy process-based machine learning methods. Natural Hazards, 1-46. https://doi.org/10.1007/s11069-025-07335-8.

Tehrany, M. S., Pradhan, B., Mansor, S., & Ahmad, N. (2015). Flood susceptibility assessment using GIS-based support vector machine model with different kernel types. Catena, 125, 91-101. https://doi.org/10.1016/j.catena.2014.10.017.

Tran, P., Shaw, R., Chantry, G., & Norton, J. (2009). GIS and local knowledge in disaster management: a case study of flood risk mapping in Viet Nam. Disasters, 33(1), 152–169. https://doi.org/10.1111/j.1467-7717.2008.01067.x.

Thammaboribal, P., Triapthti, N. K., & Lipiloet, S. (2025). Using of Analytical Hierarchy Process (AHP) in Disaster Management: A Review of Flooding and Landslide Susceptibility Mapping. International Journal of Geoinformatics, 21(4), 177-196. https://doi.org/10.52939/ijg.v21i4.4091.

Ullah, M., Murtaza, G., & Ashraf, M. (2025). Socio-Economic and Environmental Impacts of Flood 2010 in Lower Dir District and Mitigation Measures. Journal of Management & Social Science, 2(2), 556-573.

Wang, X., & Xie, H. (2018). A Review on Applications of Remote Sensing and Geographic Information Systems (GIS) in Water Resources and Flood Risk Management. Water, 10(5), 608. https://doi.org/10.3390/w10050608.

Wang, Y., Zhang, P., Xie, Y., Chen, L., & Li, Y. (2025). Toward explainable flood risk prediction: Integrating a novel hybrid machine learning model. Sustainable Cities and Society, 120, 106140. https://doi.org/10.1016/j.scs.2025.106140.

Xu, C., Rahman, M., Haase, D., Wu, Y., Su, M., & Pauleit, S. (2020). Surface runoff in urban areas: The role of residential cover and urban growth form. Journal of Cleaner Production, 262, 121421. https://doi.org/10.1016/j.jclepro.2020.121421.

Yin, Z., Hu, Y., Jenkins, K., He, Y., Forstenhäusler, N., Warren, R. & Guan, D. (2021). Assessing the economic impacts of future fluvial flooding in six countries under climate change and socio-economic development. Climatic Change, 166(3), 38. https://doi.org/10.1007/s10584-021-03059-3.

Zha, D., Bhat, Z. P., Lai, K. H., Yang, F., Jiang, Z., Zhong, S., & Hu, X. (2025). Data-centric artificial intelligence: A survey. ACM Computing Surveys, 57(5), 1-42. https://doi.org/10.1145/3711118.

Zhou, Q., Teng, S., Situ, Z., Liao, X., Feng, J., Chen, G. & Lu, Z. (2023). A deep-learning-technique-based data-driven model for accurate and rapid flood predictions in temporal and spatial dimensions. Hydrology and Earth System Sciences, 27(9), 1791-1808. https://doi.org/10.5194/hess-27-1791-2023, 2023.